Opto-Electronics Review

Symmetrical and asymmetrical imino-naphthalimides in perovskite solar cells

M. Korzec[a,*], S. Kotowicz[a], A. K. Pająk[a,b], E. Schab-Balcerzak[a,c]

[a] Institute of Chemistry, Faculty of Science and Technology, University of Silesia in Katowice, 9 Szkolna St., 40-007 Katowice, Poland
[b] Institute of Metallurgy and Materials Science, Polish Academy of Sciences, 25 Reymont St., 30-059 Krakow, Poland
[c] Centre of Polymer and Carbon Materials, Polish Academy of Sciences, 34 M. Curie-Skłodowska St., 41-819 Zabrze, Poland

Article info	Abstract
	In perovskite solar cells, series of symmetrical and asymmetrical imino-naphthalimides were tested as hole-transporting materials. The compounds exhibited high thermal stability at the temperature of the beginning of thermal decomposition above 300 °C. Obtained imino-naphthalimides were electrochemically active and their adequate energy levels confirm the application possibility in the perovskite solar cells. Imino-naphthalimides were absorbed with the maximum wavelength in the range from 331 nm to 411 nm and emitted light from the blue spectral region in a chloroform solution. The presented materials were tested in the perovskite solar cells devices with a construction of FTO/b-TiO$_2$/m-TiO$_2$/perovskite/ HTM/Au. For comparison, the reference perovskite cells were also performed (without hole-transporting materials layer). Of all the proposed materials tested as hole-transporting materials, the bis-(imino-naphthalimide) containing in core the triphenylamine structure showed a power conversion efficiency at 1.10% with a short-circuit current at 1.86 mA and an open-circuit voltage at 581 mV.

1. Introduction

1,8-Naphthalimide is a common system in the compounds with a wide range of valuable properties, used in cellular imaging, organic electronics, as well as exhibiting a broad spectrum of biological activity [1–4]. Such a broad spectrum of applications is influenced by the structure of the aromatic imide which is associated with a high electron affinity, good charge carrier mobility, high thermal and oxidative stability, as well as the ability to interact with the DNA strand (intercalation). The use of 1,8-naphthalimides in organic electronics includes both light-emitting diodes [5,6], photovoltaic cells [7–9] or field-effect tran-sistors [10]. It should be emphasized that the compounds described so far, used in organic electronics, mainly include derivatives substituted at the 4-position of the naphthalimide ring [11]. However, little is known about the physicochemical properties of 3-substituted naphthal-imides, while many reports confirm their high antitumor

activity [2,4,12,13]. According to the literature reports, the use of 4-substituted naphthalimides in perovskite solar cells (PSCs) improved devices efficiency. These compounds were used as the effective electron extraction layer [14,15]. However, triphenylamine, fluorine or biphenyl derivatives have found application as hole-transporting materials (HTMs) in the PSCs [16–20]. PSCs with the imino-triphenylamine compound acting as a hole-transporting material have showed the power conversion efficiency at 14.37% [21] and 6.68% [22]. The compounds, such as oxenates [23], thiophene-based molecules [24] or 9,9-bifluorenylidene derivative [25], were also used for PSCs as hole transporting materials with a similar device design as presented in this work. All investigated solar cells have showed approximately the same or higher efficiency (PCE), reaching a value even of 7.33% [25]. Moreover, it can be stated, that the efficiency of the developed perovskite devices, despite their low efficiency, seem to be a good alternative to other optoelectronic devices, such as bulk heterojunction solar cells (BHJ) [26–28], where various groups of chemical compounds were tested.

*Corresponding author at: mateusz.korzec@us.edu.pl

In the research carried out so far, the synthesis of a series of imino- and β-ketoenamino derivatives of 1,8-naphthalimides and the complete characteristics of these compounds, defining the scope of their use, among others in bioimaging [29] or in organic electronics, have been presented [30,31]. Research also included the synthesis and characterization of the new bis-(imino-naphthalimides) with electroluminescent properties [32].

In this paper, the research results aimed at determining the ability of synthesized symmetrical and asymmetrical imine derivatives of 1,8-naphthalimide to conduct positive charges, which were tested in perovskite photovoltaic cells, have been presented.

2. Experimental

2.1. Characterization methods

All used materials are commercially available. The NMR characterization was performed using a Bruker AC400 spectrometer 400 MHz. A Vario EL III apparatus was used to perform an elemental analysis. The absorption and emission measurements were taken on a PerkinElmer Lambda Bio 40 UV-VIS spectrometer and a Varian Carry Eclipse spectrometer. A PerkinElmer Pyris 1 TGA (heating rate of 10 °C/min and 20 cm^3/min of the nitrogen steam) was used to register thermal parameters (thermal stability from thermogravimetric analysis). Electrochemical investigations were measured using an Eco ChemieAutolab PGSTAT128n potentiostat with one-compartment cell (platinum was acting as a working electrode, 0.1 M Bu$_4$NPF$_6$ electrolyte salt in dichloromethane solution, ferrocene couple (Fc/Fc$^+$) was used as the internal standard).

2.2. PSC preparation

A fluorine doped tin oxide (FTO) glass was acting as an electrode. After cleaning, the blocking later (b-TiO$_2$) by the spin-coating method was deposited on the FTO. The mesoporous (m-TiO$_2$) layer by the screen-printed method was deposited on the blocking later. The perovskite layer was made using a two-step method. The imino-naphthalimides solutions were spin-casted on the perovskite layer, and the second electrode was a gold (Au) electrode deposited by thermal evaporation. The current-voltage characteristics (I-V) were taken using a PET Photo Emission TechInc. model SS 200AA class solar simulator. For all I-V measurements, the conditions were to achieve: 25 °C, 1000 W/m^2, AM1.5. Preparations of the PSCs are described in the paper [25].

3. Results and discussion

The compounds were obtained in a three-step reaction, starting from the available 3-nitro-1,8-naphthalic anhydride (see Fig. 1) [29–32]. In the first step, the anhydride was condensed with amines, such as hexylamine or benzylamine in the ethanol solution [Fig. 1. I)]. −NH$_2$ group was then reduced to the amine using a 10% Pd/C catalyst and hydrazine in ethanol [Fig. 1. II)]. The obtained amines were condensed with commercially available aldehydes [Fig. 1. III)], such as: 5-bromosalicylic,
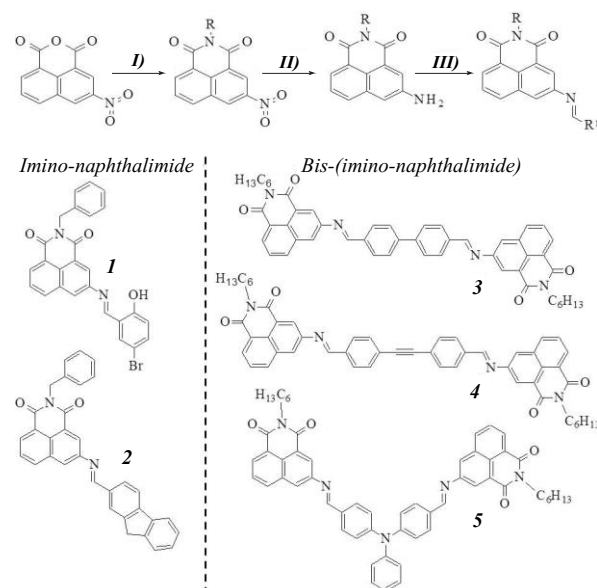

Fig. 1. Scheme of the synthesis and structure of the target compounds – naphthalimides (1–5).

9*H*-fluorene, biphenyl, triphenylamine, or a triple-bond dialdehyde [32]. The structure and purity of the presented compounds were confirmed by the ^{1}H and ^{13}C NMR analysis and an elemental analysis. Full description was given in the previous works [29–32].

The absorption (UV-Vis) and photoluminescence (PL) measurements were performed in a chloroform solution with a concentration of 10^{-5} mol/dm^3. The UV-Vis and PL spectra are presented in Fig. 2, while the data are collected in Table 1. The compounds in the chloroform solution were absorbed in the range from 270 nm to 415 nm. The absorption band with the maximum (λ_{max}) in the range of 331–345 nm corresponds to the $\pi{\rightarrow}\pi^*$ electron transition in the naphthalimide core. On the other hand, the bands with λ_{max} above 360 nm are related to the charge transfer (CT) transition between the core (at the 3-C position) and naphthalimide [30–32].
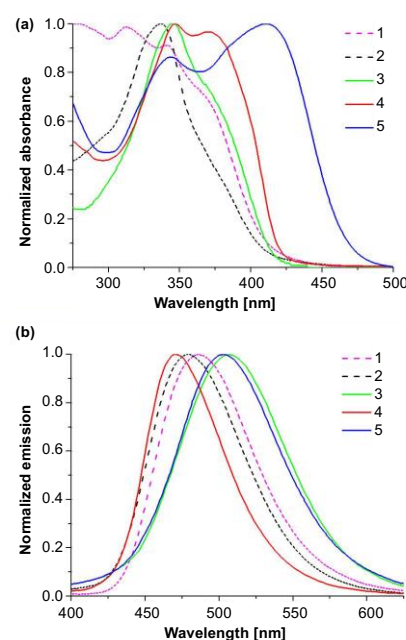

Fig. 2. UV-Vis (a) and PL spectra (b) of the 1,8-naphthalimide derivatives in the chloroform solution.

Table 1.
UV-Vis and PL properties of the imino-1,8-naphthalimides
in the chloroform solution.

Code	λ_{max} [nm] ($\varepsilon \cdot 10^4$)	E_g^{Tauc} [eV]	λ_{em} [nm]	$\Delta\lambda$ [nm]
1	331[(2.1)]; 340[(2)]	3.4	486	146
2	336[(3.9)]	3.0	478	142
3	340[(9.1)]	2.8	503	163
4	345[(9.8)]; 376[(8.8)]	2.9	470	94
5	345[(8.6)]; 411[(9.8)]	2.6	501	90

Concentration of the solutions $c = 10^{-5}$ mol/dm^3, ε is the absorption coefficient [dm^{3}mol^{-1}cm^{-1}]. λ_{em} is the emission maximum wavelength, registered for the last λ_{max}, $\Delta\lambda$ is the Stokes shift. E_g^{Tauc} is the energy band gap estimated by the Tauc method (direct band gap).

One of the materials essential properties, determining the possibility of their use in the organic electronics is the energy band gap. It can be determined, i.a., based on electronic spectra [33]. For the analysed compounds, the estimated optical energy gaps calculated using the Tauc method [34] are summarized in Table 1. In addition, the energy gaps were determined from electrochemical measurements using the cyclic voltammetry (CV) method. The compounds showed irreversible or quasi-reversible oxidation/reduction processes [30–32]. The determined energy band gap values for bis-(imino-naphthalimides) (3–5) were below 2 eV [32], while iminonaphthalimides (1, 2) had the energy bandgap above 2 eV [30,31]. This same tendency was found in the optical energy gap calculated using the Tauc method (Table 1), i.e., compounds 1 and 2 have a greater gap value than compounds 3–5.

The differences between band gaps estimated from optical absorption spectra and electrochemical measurements can be attributed to the interface barrier between the solution and the electrode [35]. The tested compounds have electrochemical energy gaps at an appropriate level to be used as components of PSCs.

Thermal studies of the obtained 1,8-naphthalimide derivatives were performed using thermogravimetry (TG). The compounds showed high thermal stability, determined based on a temperature of a 5% weight loss ($T_{5\%}$). For compounds 3–5 (Fig. 1) [32], the $T_{5\%}$ temperature was: 387 °C (3), 285 °C (4) and 426 °C (5) (see Fig. 3). On the other hand, unsymmetrical naphthalimides showed stability above 300 °C [30,31].
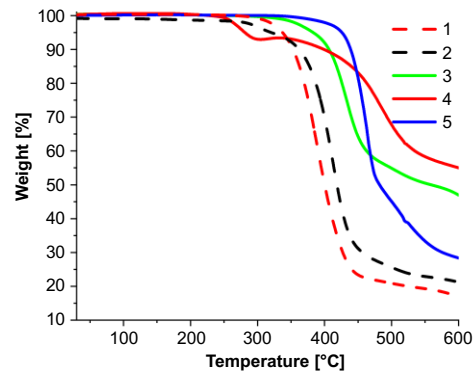

Fig. 3. TGA thermograms of the compounds 1–5.

The synthesized 1,8-naphthalimide derivatives were tested as holes transporting materials (HTMs) in the PSCs. The two types of devices were prepared: the reference solar cell without HTM layer and devices with a sandwich configuration: FTO/b-TiO$_2$/m-TiO$_2$/perovskite/HTM/Au (Fig. 4). Determined photovoltaic parameters based on the current-voltage (I-V) characteristics of the solar cells are presented in Table 2. The perovskite layer was obtained
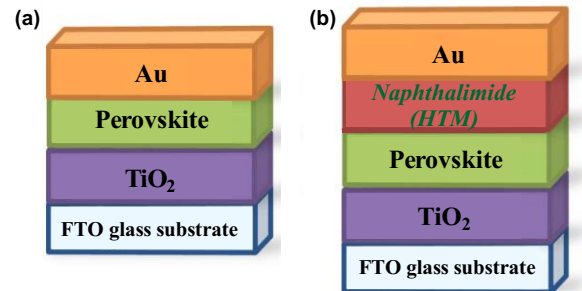

Fig. 4. Sandwich configuration of the prepared PSCs: reference cell (a) and with HTM layer (b).

Table 2.
Photovoltaic parameters of the tested perovskite solar cells.

Device structure	I_{sc} [mA]	J_{sc} [mA/cm^2]	V_{oc} [mV]	FF [–]	PCE [%]	IP	EA	E_g
FTO/b-TiO$_2$/m-TiO$_2$/perovskite/Au	0.45[1] ± 0.01 0.36[2] ± 0.04	1.79[1] ± 0.02 1.42[2] ± 0.14	202[1] ± 24 217[2] ± 17	0.26[1] ± 0.00 0.25[2] ± 0.00	0.10[1] ± 0.02 0.08[2] ± 0.01	–	–	–
FTO/b-TiO$_2$/m-TiO$_2$/perovskite/1/Au	0.80[1] ± 0.07 0.59[2] ± 0.01	3.20[1] ± 0.28 2.35[2] ± 0.03	598[1] ± 20 626[2] ± 19	0.34[1] ± 0.01 0.30[2] ± 0.00	0.68[1] ± 0.06 0.47[2] ± 0.03	−6.29	−3.58	2.71
FTO/b-TiO$_2$/m-TiO$_2$/perovskite/2/Au	0.68[1] ± 0.00 0.67[2] ± 0.02	2.73[1] ± 0.02 2.68[2] ± 0.07	540[1] ± 21 494[2] ± 49	0.32[1] ± 0.01 0.26[2] ± 0.00	0.50[1] ± 0.03 0.36[2] ± 0.04	−5.72	−3.37	2.35
FTO/b-TiO$_2$/m-TiO$_2$/perovskite/3/Au	0.29[1] ± 0.01 0.24[2] ± 0.01	1.14[1] ± 0.05 0.96[2] ± 0.03	699[1] ± 62 710[2] ± 4	0.40[1] ± 0.05 0.39[2] ± 0.04	0.33[1] ± 0.07 0.28[2] ± 0.03	−5.51	−3.72	1.79
FTO/b-TiO$_2$/m-TiO$_2$/perovskite/4/Au	0.10[1] ± 0.01 0.07[2] ± 0.00	0.39[1] ± 0.06 0.29[2] ± 0.01	689[1] ± 27 633[2] ± 1	0.37[1] ± 0.03 0.35[2] ± 0.01	0.10[1] ± 0.02 0.07[2] ± 0.00	−5.80	−3.83	1.97
FTO/b-TiO$_2$/m-TiO$_2$/perovskite/5/Au	1.86[1] ± 0.03 2.16[2] ± 0.18	7.44[1] ± 0.11 8.63[2] ± 0.73	581[1] ± 14 591[2] ± 53	0.24[1] ± 0.01 0.15[2] ± 0.00	1.10[1] ± 0.02 0.83[2] ± 0.15	−5.63	−3.87	1.76

I_{sc} is the short-circuit current, J_{sc} is the short-circuit current density, V_{oc} is the open-circuit voltage, FF is the fill factor, PCE is the efficiency of a photovoltaic cell, [1]forward scan, [2]backward scan. Cells active area is of 0.25 cm^2. IP (ionization potential) and EA (electron affinities) taken from cyclic voltammetry. IP $= -5.1 - E_{ox(onset)} \cdot |e^-|$, EA $= -5.1 - E_{red(onset)} \cdot |e^-|$, $E_g = E_{ox(onset)} - E_{red(onset)}$.

using a two-step method [25]. HTM layer was doped with lithium bis-(trifluoromethanesulfonyl) imide (Li-TFSI) at a concentration of 17.5 μL. Li-TFSI is a common *p*-dopant of the hole transport layer which increases the conductivity [36].

Measurements were carried out under standard conditions (STC). Active area of the tested cells was of 0.25 cm^2. Presented results were obtained for the champion device from measurements of five series of devices. Solar cell containing a 1,8-naphthalimide derivative with the triphenylamine structure 5 was characterized by the highest conversion efficiency (PCE = 1.10%) and the highest J_{sc} (1.86 mA) and V_{oc} (581 mV), I-V characteristic is presented in Figs. 5–7. Solar cells, in which the synthesized compounds were tested, showed higher PCE values compared to the reference cell, except for the 1,8-naphthalimide imine derivative with an ethynyl bridge (4). An increase in the open circuit voltage was observed for all devices compared to the solar cell without HTM, which may indicate low voltage losses at the junction (Table 2). The forward and backward electrical measurements allow to observe the I-V hysteresis. An important issue is to understand and counteract the hysteresis behaviour which is confirmed by many scientific papers focusing on understanding this phenomenon [37]. In the forward scans, the PCE was higher than in the backward scans, and the differences between PCE from forward and backward measurements were in the range from 0.03% to 0.27%. The device with compound 5 (acting as HTM) exhibited the highest conversion efficiency in the forward scan and at the same time, the biggest difference between both scans (ΔPCE = 0.27%). The understanding of the doping mechanism is also an important factor. Considering the literature data, the reactions involved in the doping process are discussed with regard to a spiro-OMeTAD doped with Li$^+$TFSI$^-$ [38]. Abate *et al*. [39] claim that the pristine spiro-OMeTAD reacts with O_2 after exposition of the thin film to air or heat and a weakly bound complex is formed. The TFSI$^-$ anion stabilizes the oxidized Spiro-OMeTAD. The rest of the lithium ions (Li$^+$) can react with oxygen ($O_2^{\cdot-}$). A spectrum-dependent mechanism for oxidation of Spiro-OMeTAD with LiTFSI was proposed by Wang *et al*. [40]. Even though the doping mechanism in the case of Spiro-MeOTAD was examined, some questions are still not resolved. Based on the compounds described in this paper, during the oxidation process, radical cations were produced, and two possible doping mechanisms can occur (proposed mechanism for compound 5 with a donor TPA group):

1) $HTM5(TPA) + O_2 \rightarrow HTM5(TPA)^{\cdot+}O_2^{\cdot-}$
   $HTM5(TPA)^{\cdot+}O_2^{\cdot-} + Li^+TFSI^- \rightarrow$
   $HTM5(TPA)^{\cdot+}TFSI^- + Li_xO_y$

2) $Perovskite + O_2 \rightarrow Perovskite^{\cdot+}O_2^{\cdot-}$
   $Perovskite^{\cdot+}O_2^{\cdot-} + HTM5(TPA) \rightarrow$
   $Perovskite + HTM5(TPA)^{\cdot+}O_2^{\cdot-}$
   $HTM5(TPA)^{\cdot+}O_2^{\cdot-} + Li^{\cdot+}TFSI^- \rightarrow$
   $HTM5(TPA)^{\cdot+}TFSI^- + Li_xO_y$

It should be stressed that it is only a proposed mechanism and for its confirmation further investigations are needed.
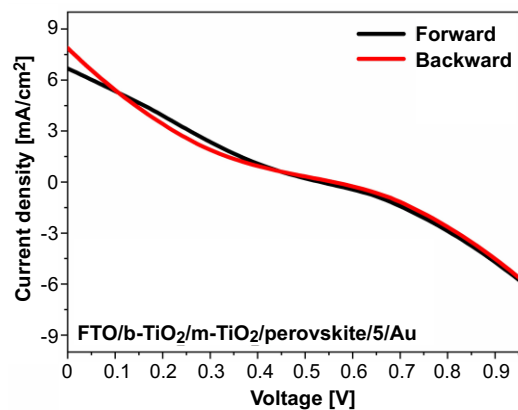

Fig. 5. I-V characteristic of the PSC device with compound 5 as a hole transporting material.
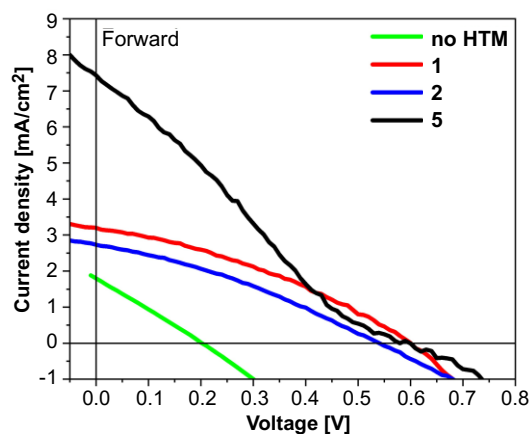

Fig. 6. I-V characteristic of the PSC devices without HTM and with compounds 1,2,5 in forward scan.
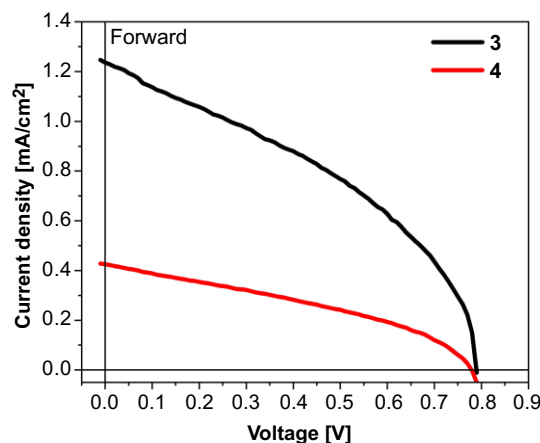

Fig. 7. I-V characteristic of the PSC devices with compounds 3 and 4 in forward scan.

4. Conclusions

The symmetrical and asymmetrical imine derivatives of 1,8-naphthalimide, whose ability to transport positive charges was tested in the PSCs, is presented in this paper. Also, synthesis, thermal, electrochemical, and optical properties in the chloroform solution which were the subject of several previous works devoted to these compounds are presented here. The influence of the chemical structure on properties, including the ability to

electroluminescence (structures 3–5) [32] and, as shown in this paper, the possibility to act as a hole transporting material, was observed. Based on the photovoltaic parameters, it can be concluded that the presence of thetriphenylamine structure 5 has a beneficial effect on the PCE values.

Authors' statement

Research concept and design, M. K. and E. S.-B., collection and/or assembly of data A. K. P., data analysis and interpretation, M. K., S. K., and A. K. P., writing of the article, M. K., critical revision of the article, S. K. and E. S.-B., final approval of the article, M. K. and S. K.

Acknowledgements

References

[1] Gopikrishna, P., Meher, N. & Iyer P. K. Functional 1,8-naphthalimide AIE/AIEEgens: recent advances and prospects. *ACS Appl. Mater. Interfaces* **10**, 12081–12111 (2018). https://doi.org/10.1021/acsami.7b14473

[2] Banerjee, S. *et al*. Recent advances in the development of 1,8-naphthalimide based DNA targeting binders, anticancer and fluorescent cellular imaging agents. *Chem. Soc. Rev.* **42**, 1601–1618 (2013). https://doi.org/10.1039/C2CS35467E

[3] Poddar, M., Sivakumar, G. & Misra, R. Donor-acceptor substituted 1,8-naphthalimides: design, synthesis, and structure–property relationship *J. Mater. Chem. C* **7**, 14798–14815 (2019). https://doi.org/10.1039/C9TC02634G

[4] Tomczyk, M. D. & Walczak K. Z. l,8-Naphthalimide based DNA intercalators and anticancer agents. A systematic review from 2007 to 2017. *Eur. J. Med. Chem.* **159**, 393–422 (2018). https://doi.org/10.1016/j.ejmech.2018.09.055

[5] Gan, J.-A. *et al*. 1,8-naphthalimides for non-doping OLEDs: the tunable emission color from blue, green to red. *J. Photochem. Photobiol.* **162**, 399–406 (2004). https://doi.org/10.1016/S1010-6030(03)00381-2

[6] Luo, S. *et al*. Novel 1,8-naphthalimide derivatives for standard-red organic light-emitting device applications. *J. Mater. Chem. C* **3**, 525–5267 (2015). https://doi.org/10.1039/C5TC00409H

[7] Zhang, X. *et al*. A 1,8-naphthalimide based small molecular acceptor for polymer solar cells with high open circuit voltage, *J. Mater. Chem. C* **3**, 6979–6985 (2015). https://doi.org/10.1039/C5TC01148E

[8] Do, T. T. *et al*. Molecular engineering strategy for high efficiency fullerene-free organic solar cells using conjugated 1,8-naphthalimide and fluorenone building blocks. *ACS Appl. Mater. Interfaces* **9**, 16967–16976 (2017). https://doi.org/10.1021/acsami.6b16395

[9] Yadagiri, B. *et al*. An all-small-molecule organic solar cell derived from naphthalimide for solution-processed high-efficiency non-fullerene acceptors. *J. Mater. Chem. C* **7**, 709–717 (2019). https://doi.org/10.1039/C8TC05692G

[10] Torres-Moya, I. *et al*. Synthesis of D-π-A high-emissive 6-arylalkynyl-1,8-naphthalimides for application in organic field-effect transistors and optical waveguides *Dyes and Pigm.* **191**, 109358 (2021). https://doi.org/10.1016/j.dyepig.2021.109358

[11] Gudeika, D. A review of investigation on 4-substituted 1,8-naphthalimide derivatives. *Synth. Met.* **262**, 116328 (2020). https://doi.org/10.1016/j.synthmet.2020.116328

[12] Xie, L. *et al*. 5-Non-amino aromatic substituted naphthalimides as potential antitumor agents: Synthesis via Suzuki reaction, antiproliferative activity, and DNA-binding behavior. *Bioorg. Med. Chem.* **19**, 961–967 (2011). https://doi.org/10.1016/j.bmc.2010.11.055

[13] Rykowski, S. *et al*. Design, synthesis, and evaluation of novel 3-carboranyl-1,8-naphthalimide derivatives as potential anticancer agents. *Int. J. Mol. Sci.* **22**, 2772 (2021). https://doi.org/10.3390/ijms22052772

[14] Sivakumar, G. *et al*. Design, synthesis and characterization of 1,8-naphthalimide based fullerene derivative as electron transport material for inverted perovskite solar cells. *Synth. Met.* **249**, 25–30 (2019). https://doi.org/10.1016/j.synthmet.2019.01.014

[15] Li, L. *et al*. Self-assembled naphthalimide derivatives as an efficient and low-cost electron extraction layer for n-i-p perovskite solar cells. *Chem. Commun.* **55**, 13239–13242 (2019). https://doi.org/10.1039/C9CC06345E

[16] Agarwala, P. & Kabra, D. A review on triphenylamine (TPA) based organic hole transport materials (HTMs) for dye sensitized solar cells (DSSCs) and perovskite solar cells (PSCs): evolution and molecular engineering. *J. Mater. Chem. A* **5**, 1348–1373 (2017). https://doi.org/10.1039/C6TA08449D

[17] Duan, L. *et al*. Facile synthesis of triphenylamine-based hole-transporting materials for planar perovskite solar cells. *J. Power Sources* **435**, 226767 (2019). https://doi.org/10.1016/j.jpowsour.2019.226767

[18] Wu, G. *et al*. Triphenylamine-based hole transporting materials with thiophene-derived bridges for perovskite solar cells. *Synth. Met.* **261**, 116323 (2020). https://doi.org/10.1016/j.synthmet.2020.116323

[19] Rezaei, F. & Mohajeri, A. Molecular designing of triphenylamine-based hole-transporting materials for perovskite solar cells *Sol. Energy* **221**, 536–544 (2021). https://doi.org/10.1016/j.solener.2021.04.055

[20] Li, M. *et al*. Facile donor (D)-π-D triphenylamine-based hole transporting materials with different π-linker for perovskite solar cells. *Sol. Energy* **195**, 618–625 (2020). https://doi.org/10.1016/j.solener.2019.11.071

[21] Bogdanowicz, K. A. *et al*. Selected electrochemical properties of 4,4'-((1E,1'E)-((1,2,4-Thiadiazole-3,5-diyl)bis(azaneylylidene))-bis(methaneylylidene))bis(N,N-di-p-tolylaniline) towards perovskite solar cells with 14.4% efficiency. *Materials* **13**, 2440 (2020). https://doi.org/10.3390/ma13112440

[22] Ma, B.-B. *et al*. Visualized acid–base discoloration and optoelectronic investigations of azines and azomethines having double 4-[*N,N*-di(4-methoxyphenyl)amino]phenyl terminals. *J. Mater. Chem. C* **3**, 7748–7755 (2015). https://doi.org/10.1039/C5TC00909J

[23] Korzec, M. *et al*. Synthesis and thermal, photophysical, electrochemical properties of 3,3-di[3-arylcarbazol-9-ulmethyl]oxetane derivatives. *Materials* **14**, 5569 (2021). https://doi.org/10.3390/ma14195569

[24] Pająk, A. K. *et al*. New thiophene imines acting as hole transporting materials in photovoltaic devices. *Energy Fuels* **34**, 10160–10169 (2020). https://doi.org/10.1021/acs.energyfuels.0c01698

[25] Kula, S. *et al*. 9,9'-bifluorenylidene derivatives as novel hole-transporting materials for potential photovoltaic applications. *Dyes Pigm.* **174**, 108031 (2020). https://doi.org/10.1016/j.dyepig.2019.108031

[26] Derkowska-Zielinska, B. *et al*. Photovoltaic cells with various azo dyes as components of the active layer. *Sol. Energy* **203**, 19–24 (2020). https://doi.org/10.1016/j.solener.2020.04.022

[27] Nitschke, P. *et al*. Spectroscopic and electrochemical properties of thiophene-phenylene based Schiff-bases with alkoxy side groups, towards photovoltaic applications. *Spectrochim. Acta A* **248**, 119242 (2021). https://doi.org/10.1016/j.saa.2020.119242

[28] Sęk, D. *et al*. Polycyclic aromatic hydrocarbons connected with Schiff base linkers: Experimental and theoretical photophysical characterization and electrochemical properties *Spectrochim. Acta A,* **175**, 168–176 (2017). https://doi.org/10.1016/j.saa.2016.12.029

[29] Korzec, M. *et al*. Live cell imaging by 3-imino-(2-phenol)-1,8-naphthalimides: The effect of ex vivo hydrolysis. *Spectrochim. Acta A* **238**, 118442 (2020). https://doi.org/10.1016/j.saa.2020.118442

[30] Kotowicz, S. *et al*. Novel 1,8-naphthalimides substituted at 3-C position: Synthesis and evaluation of thermal, electrochemical and luminescent properties. *Dyes Pigm.* **158**, 65–78 (2018). https://doi.org/10.1016/j.dyepig.2018.05.017

[31] Korzec, M. *et al*. Novel b-ketoenamines versus azomethines for organic electronics: characterization of optical and electrochemical properties supported by theoretical studies. *J Mater Sci*, **55**, 3812–3832 (2020). https://doi.org/10.1007/s10853-019-04210-3

[32] Kotowicz, S. *et al*. New acceptor–donor–acceptor systems based on bis-(imino-1,8-naphthalimide). *Materials* **14**, 2714 (2021). https://doi.org/10.3390/ma14112714

[33] Costa, J. S. C. *et al*. Optical band gaps of organic semiconductor materials *Opt. Mater.* **58**, 51–60 (2016). https://doi.org/10.1016/j.optmat.2016.03.041

[34] Nitschke, P. *et al*. The effect of alkyl substitution of novel imines on their supramolecular organization, towards photovoltaic applications, *Sol. Energy* **221**, 536–544. https://doi.org/10.1016/j.solener.2021.04.055

[35] Misra, A. *et al*. Electrochemical and optical studies of conjugated polymers for three primary colours. *Indian J. Pure Appl. Phys.* **43**, 921–925 (2005).

[36] Kim, K. *et al*. Direct p-doping of Li-TFSI for efficient hole injection: Role of polaronic level in molecular doping. *Appl. Surf. Sci.* **480**, 565–571 (2019). https://doi.org/10.1016/j.apsusc.2019.02.248

[37] Singh, R. & Parashar, M. *Origin of Hysteresis in Perovskite Solar Cells in Soft-Matter Thin Film Solar Cells: Physical Processes and Device Simulation* (AIP Publishing, on-line) (New York, 2020). https://doi.org/10.1063/9780735422414_001

[38] Li, B. *et al*. Insights into the hole transport properties of LiTFSI-doped spiro-OMeTAD films through impedance spectroscopy. *J. Appl. Phys.* **128**, 085501 (2020). https://doi.org/10.1063/5.0011868

[39] Abate, A. *et al*. Lithium salts "redox active" *p*-type dopants for organic semiconductors and their impact in solid-state dye-sensitized solar cells. *Phys. Chem. Chem. Phys.*, **15**, 2572–2579 (2013). https://doi.org/10.1039/C2CP44397J

[40] Wang, S., Yan, W. & Meng, Y. S., Spectrum-dependent spiro-OMeTAD oxidization mechanism in perovskite solar cells. *Appl. Mater. Interfaces* **7**, 24791–24798 (2015). https://doi.org/10.1021/acsami.5b07703